Supplementary Materials

Composited analyses of the chemical and physical characteristics of co-polluted days by ozone and $PM_{2.5}$ over 2013-2020 in the Beijing–Tianjin–Hebei region

Huibin Dai[1], Hong Liao[1*], Ke Li[1], Xu Yue[1], Yang Yang[1], Jia Zhu [1], Jianbing Jin[1], Baojie Li[1]

[1]Jiangsu Key Laboratory of Atmospheric Environment Monitoring and Pollution Control, Jiangsu Collaborative Innovation Center of Atmospheric Environment and Equipment Technology, School of Environmental Science and Engineering, Nanjing University of Information Science & Technology, Nanjing 210044, China

*Correspondence to: Hong Liao (hongliao@nuist.edu.cn)

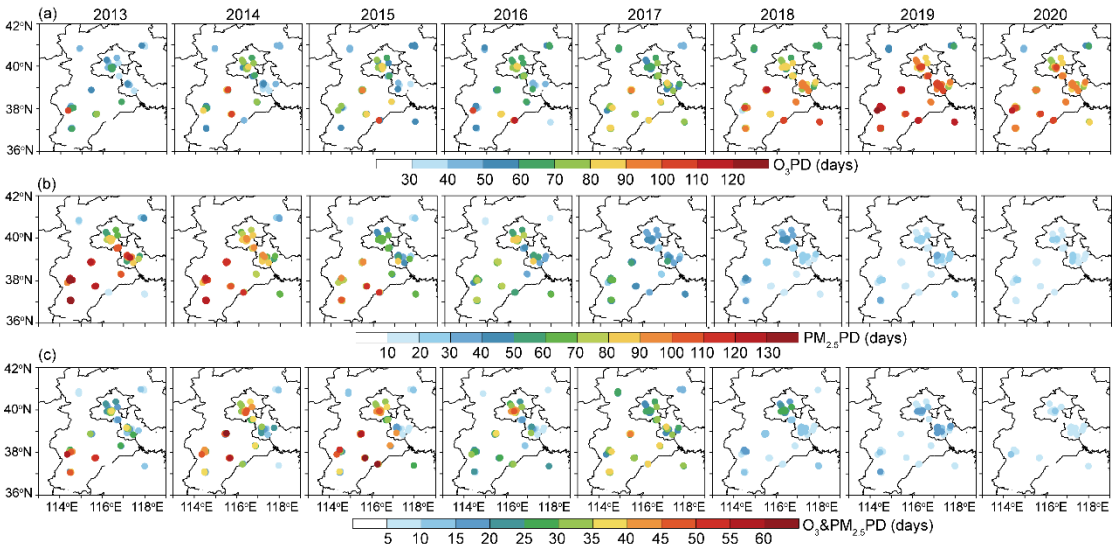

Figure S1. Spatial distributions of observed numbers of (a) O_3PD (MDA8 O_3 > 80 ppb), (b) $PM_{2.5}$PD ($PM_{2.5}$ > 75 μg m^{-3}), and (c) O_3&$PM_{2.5}$PD (MDA8 O_3 > 80 ppb and $PM_{2.5}$ > 75 μg m^{-3}) summed over April-October from 2013 to 2020 in BTH.

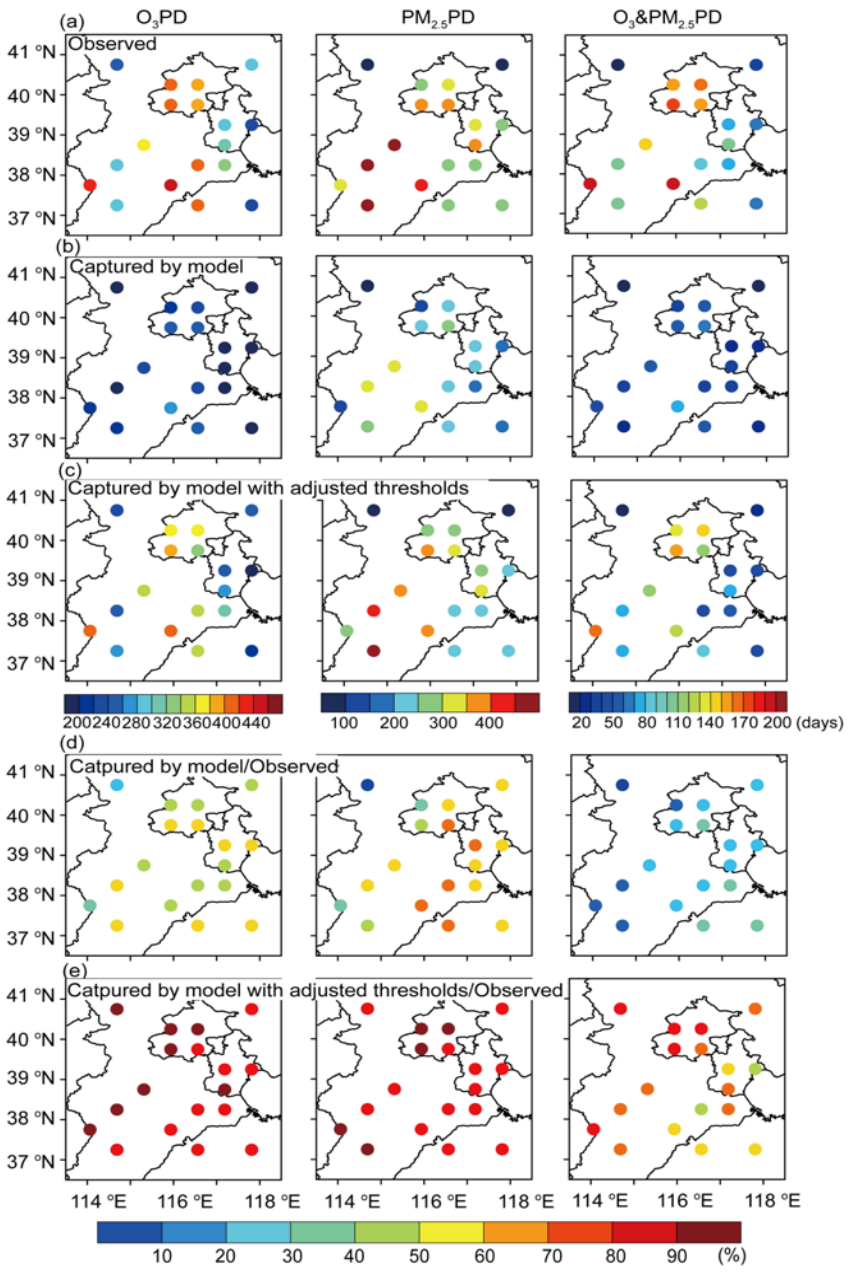

Figure S2. Spatial distributions of (a) observed numbers of O_3SPD, $PM_{2.5}$SPD, and O_3&$PM_{2.5}$PD, (b) numbers of polluted days captured by the GEOS-Chem model with the threshold of 80 ppb for MDA8 O_3 and 75 μg m^{-3} for $PM_{2.5}$ and (c) numbers of polluted days captured by the GEOS-Chem model with adjusted thresholds. Percentage of polluted days (d) captured by the model and (e) captured by the model with adjusted thresholds. The values were calculated for the warm months (April to October) of 2013-2020.

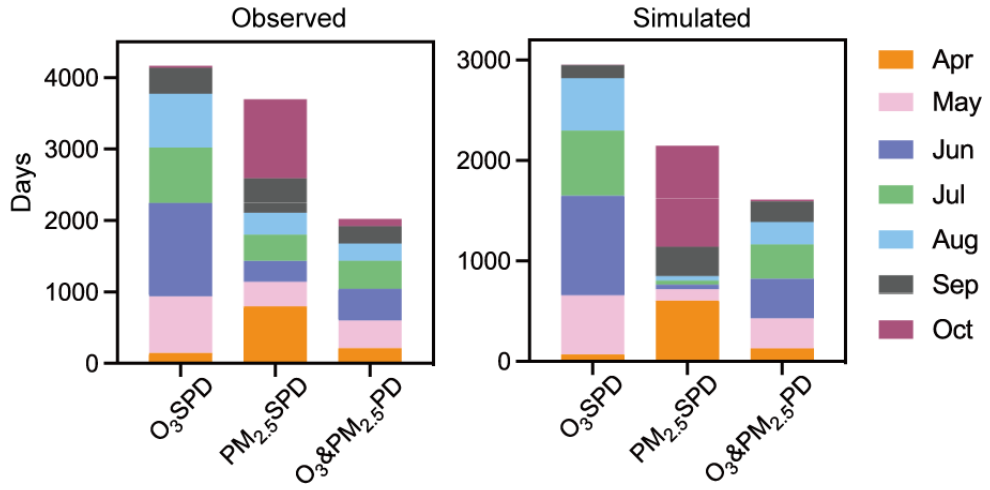

Figure S3. The observed and model-captured numbers of O_3SPD, $PM_{2.5}$SPD, O_3&$PM_{2.5}$PD in each month summed over 2013-2010 in BTH.

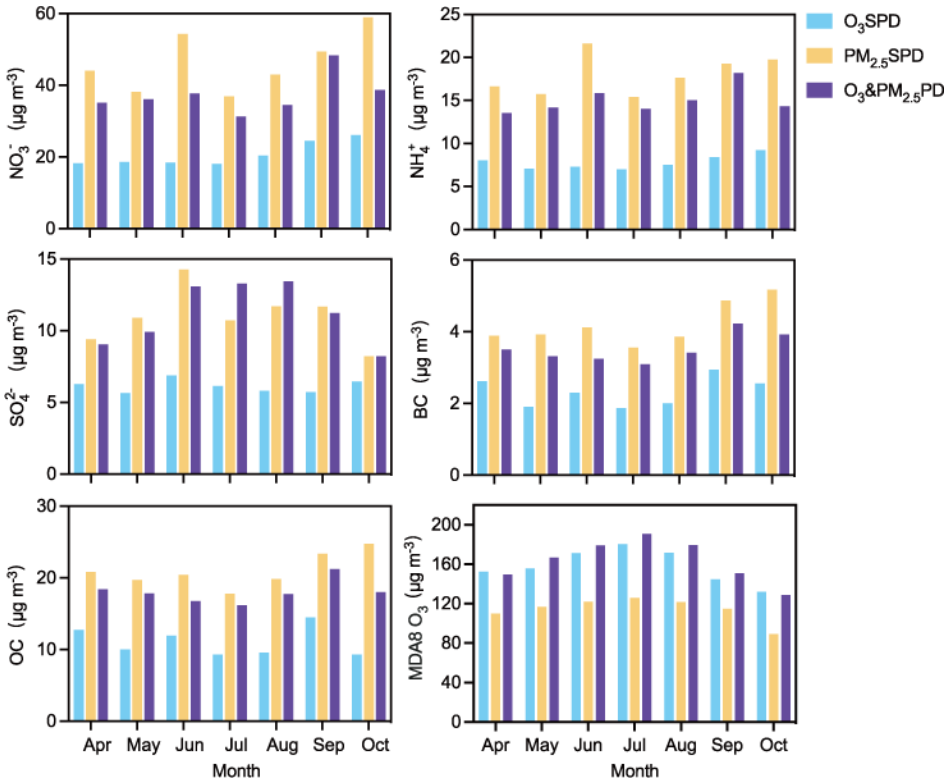

Figure S4. The concentrations of $PM_{2.5}$ components (μg m^{-3}): NO_3^-, NH_4^+, SO_4^{2-}, BC, and OC as well as MDA8 O_3 averaged in model-captured O_3SPD, $PM_{2.5}$SPD, and O_3&$PM_{2.5}$PD over BTH in each month of 2013-2020.

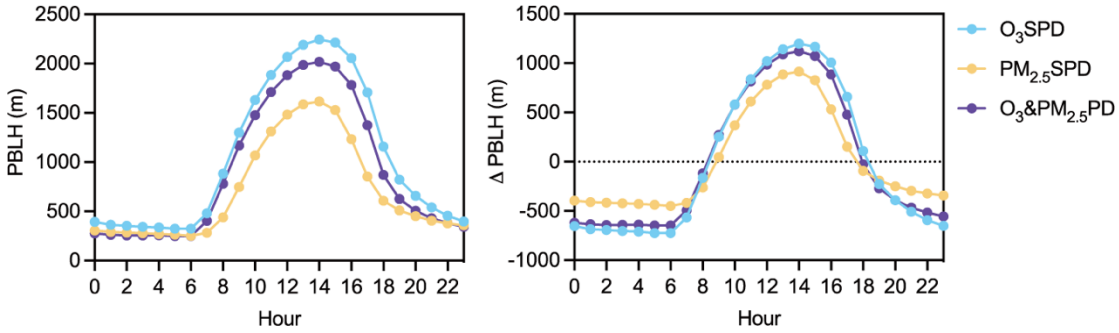

Figure S5. The hourly variations of PBLH (m) and ΔPBLH (daily anomaly of PBLH, m) averaged in all model-captured O_3SPD (blue), $PM_{2.5}$SPD (yellow), and O_3&$PM_{2.5}$PD (purple) over the warm months (April-October) of 2013-2020.

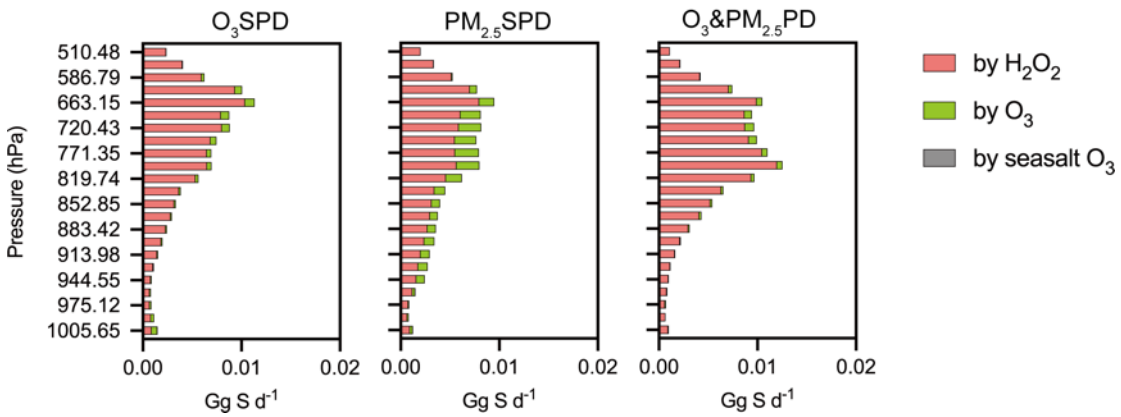

Figure S6. The vertical profile of SO_4^{2-} chemical production ($P(SO_4^{2-})$, Gg S d^{-1}) from aqueous oxidation of H_2O_2 in clouds, aqueous oxidation of O_3 in clouds, and O_3 on sea salt aerosols over BTH. The values were averaged over the model-captured regional O_3SPD, $PM_{2.5}$SPD, and O_3&$PM_{2.5}$PD in April-October of 2013-2020.

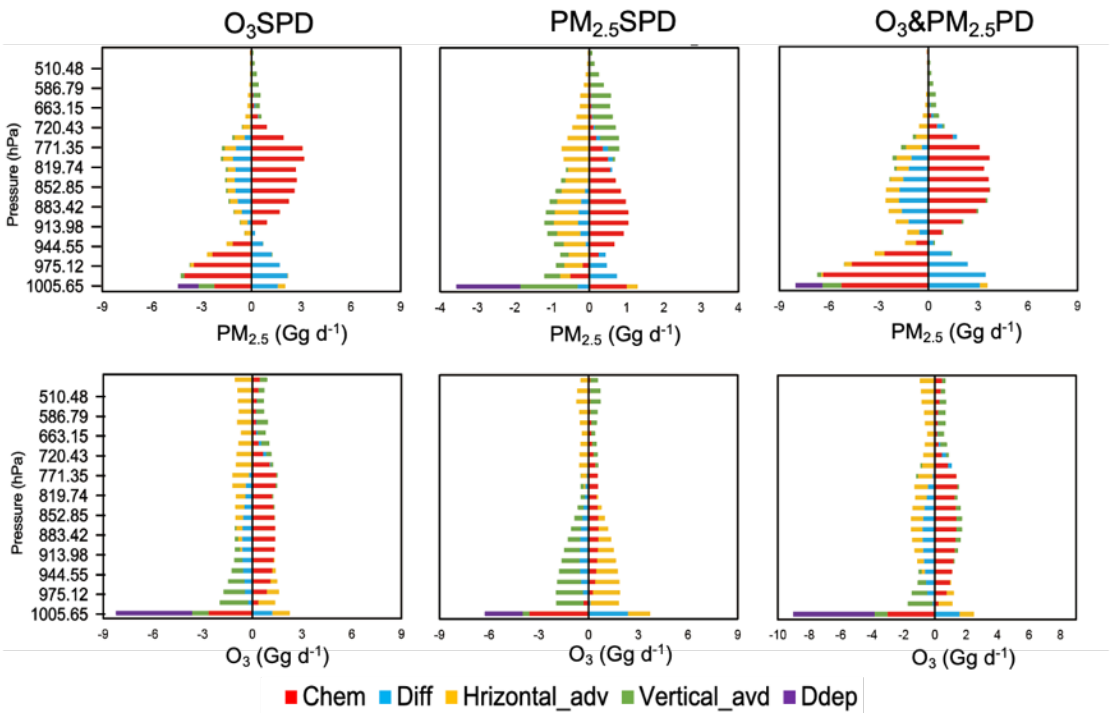

Figure S7. The vertical profile of net change in the total of $PM_{2.5}$ components mass (NO_3^- + NH_4^+ + SO_4^{2-} + OC, Gg d^{-1}) and O_3 mass (Gg d^{-1}) over BTH for each process. The values were averaged over the model-captured regional O_3SPD, $PM_{2.5}$SPD, and O_3&$PM_{2.5}$PD in April-October of 2013-2020.

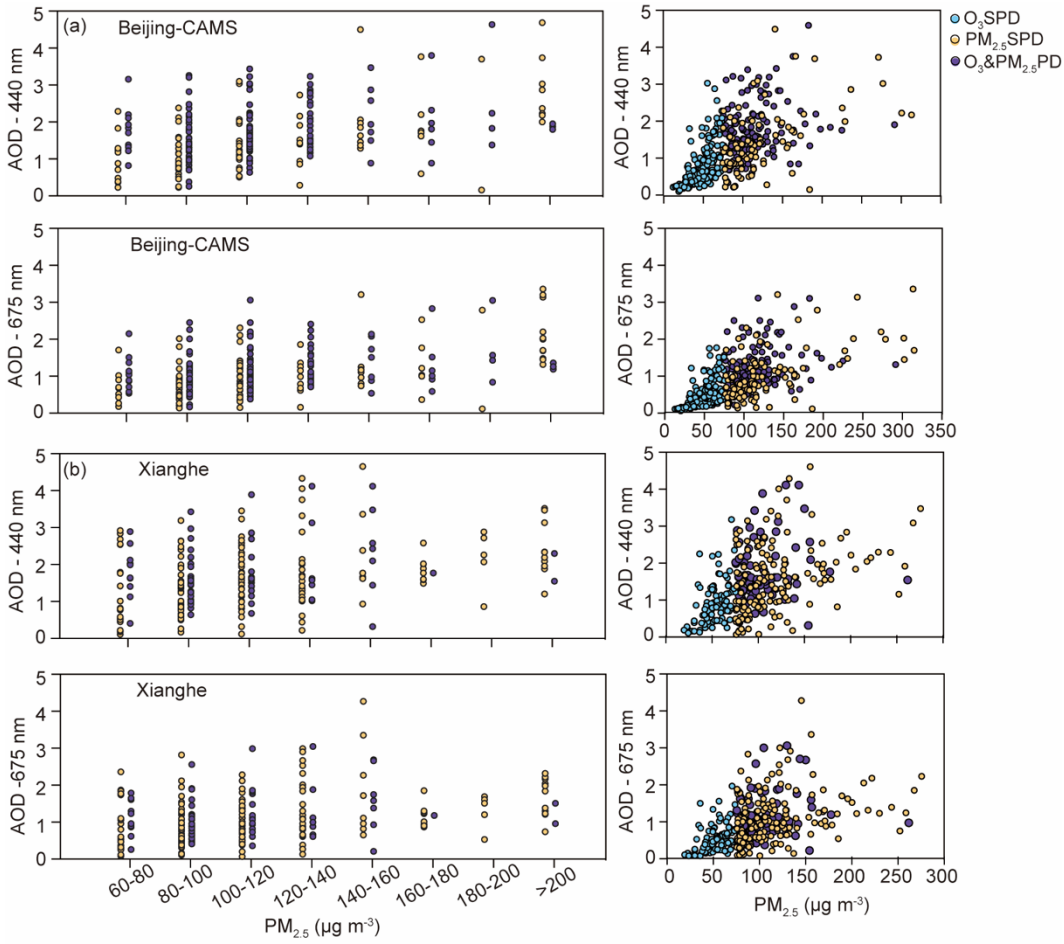

Figure S8. The same as Figure. 10 but for Beijing-CAMS and Xianghe station.

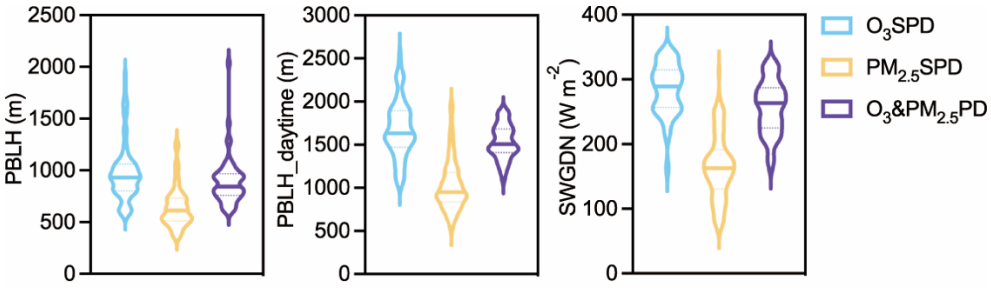

Figure S9. The violin plot of planetary boundary layer height (PBLH, m), daytime planetary boundary layer height (PBLH_daytime, m), surface incoming shortwave flux (SWGDN, W m^{-2}) in model-captured O_3SPD (blue), $PM_{2.5}$SPD (yellow), and O_3&$PM_{2.5}$PD (purple) in the months of April to October from 2013-2020. The solid line in the middle represents the median value.

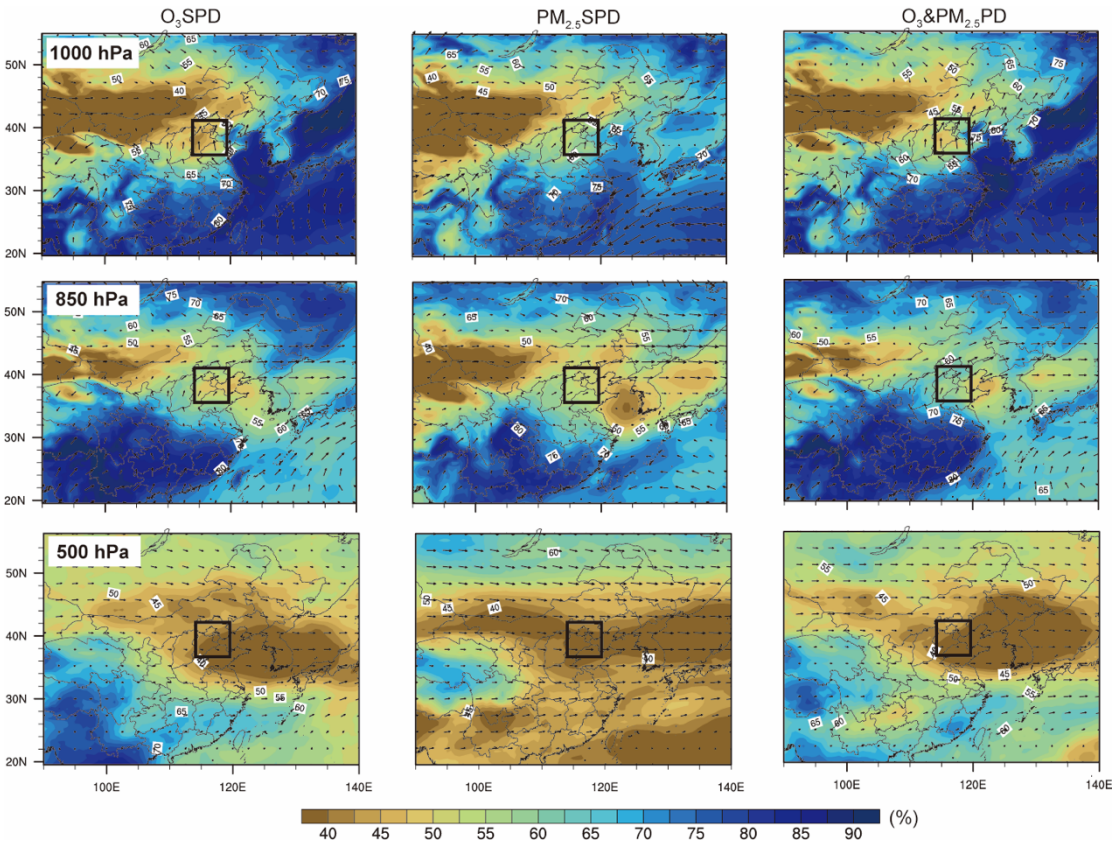

Figure S10. Composites of wind field (m s^{-1}) with RH (%) at 1000 hPa, 850 hPa and 500 hPa for regional O_3SPD, $PM_{2.5}$SPD, and O_3&$PM_{2.5}$PD that were captured by the model in April-October of 2013-2020. The solid black lines indicate BTH region.